2nd International Joint Conference on Water Distribution Systems Analysis & Computing and Control in the Water Industry
Valencia (Spain), 18-22 July 2022
doi: https://doi.org/10.4995/WDSA-CCWI2022.2022.14005

INVESTIGATING AN ALTERNATIVE TO EXHUMED GREY CAST IRON WATER PIPES FOR SMALL-SCALE FATIGUE TESTS

Edward John[1], Joby Boxall[2], Richard Collins[3], Elisabeth Bowman[4], and Luca Susmel[5]

[1,2,3,4,5]Department of Civil and Structural Engineering, The University of Sheffield, Sheffield, UK

[1] *edajohn1@sheffield.ac.uk*, [2] *j.b.boxall@sheffield.ac.uk*, [3] *r.p.collins@sheffield.ac.uk*, [4] *e.bowman@sheffield.ac.uk*, [5] *l.susmel@sheffield.ac.uk*

Abstract

Reducing and preventing leakage is a priority for water distribution network managers in many countries, including the UK. Understanding the mechanisms that cause leaks to form, and developing the ability to model these processes, will enable proactive replacement of water pipes before they start to leak. Smaller diameter Grey Cast Iron (GCI) water pipes are understood to experience biaxial, repeating loads, so fatigue cracking may be a cause of leakage for these pipes. To investigate this fatigue cracking mechanism a small-scale biaxial fatigue experiment is under development at The University of Sheffield. A large number of small diameter, un-corroded GCI pipes are needed to serve as specimens for this experiment. Therefore, in this work off-the-shelf BS416-2 DN 50 mm soil pipes are explored as an alternative to using exhumed pipes, which are often corroded and ≥76.2 mm diameter. The graphite microstructure and tensile stress-strain behaviour of a BS416-2 pipe were characterised and compared with literature data for exhumed spun-cast GCI water pipes, and a good agreement was found. This work concluded that BS 416-2 soil pipes can be used to represent spun-cast GCI water pipes in small-scale destructive experiments.

Keywords
Water distribution pipe, grey cast iron, leakage, material properties, graphite microstructure.

1 INTRODUCTION

Reducing and preventing leakage is a priority for water distribution network managers in many countries, including the UK. Understanding the mechanisms that cause leaks to form, and developing the ability to model these processes, will enable proactive replacement of water pipes before they start to leak. Grey Cast Iron (GCI) pipes are amongst the oldest pipes still in service, most having been installed pre-1960, and are still common in many UK networks [1]. One way that GCI pipes can develop leaks is by forming through-wall cracks [2].

Smaller diameter GCI pipes experience biaxial stress states; internal water pressure causes a pipe to experience stress acting around its circumference [3] and bending loads, such as vehicles and soil response to moisture change, cause stress acting in the pipe's axial direction [4], [5]. These loads are time variable with the potential to cycle tens or even hundreds of times per day [6], [7].

Developing a fundamental understanding of how GCI pipes develop through-wall cracks in response to these loads must be done experimentally so that the loading can be controlled, tests can be repeated, and the failure mode can be observed. For example, the formation of fatigue cracks in GCI pipes has been proposed as a potential leak initiation mechanism [8], [9], but physical tests are needed to confirm this and validate a suitable fatigue failure criterion. These tests must include cyclic, biaxial stress conditions to investigate the effect of this loading type on the time it takes for a leaking crack to form. However, no process or equipment has previously been developed that can apply cyclic, biaxial stresses to a GCI water pipe.

A small-scale experiment that is capable of fatigue testing GCI pipes using biaxial stress histories is under development at the University of Sheffield to investigate the fatigue cracking leakage mechanism. For the specimens in this experiment, small diameter, un-corroded GCI pipes are needed. Smaller diameter pipes require lower bending loads to generate a given stress magnitude, enabling higher loading frequencies and shorter test durations. Using un-corroded pipes means artificial corrosion pit geometries can be added in a controlled way. Exhumed pipes are typically ≥76.2 mm nominal diameter and in variable states of deterioration, sometimes featuring deep corrosion pits or through-wall cracks [10], [11]. Newly manufactured GCI water pipes without corrosion would be more suitable but unfortunately new GCI water pipes are no longer widely manufactured because ductile iron, steel, and plastic pipes are used in new installations [1]. A potential alternative to new GCI water pipes is off-the-shelf soil pipes made in accordance with BS 416-2, which are easy to obtain, manufactured from GCI, and available with nominal diameters from 50 mm to 150 mm [12].

The work presented in this paper investigates whether BS 416-2 soil pipes can be used to represent GCI water pipes in small-scale destructive experiments where small diameter, un-corroded pipes are needed. Two aspects were considered in this investigation: the pipe's graphite microstructure, and the pipe's tensile stress-strain response. The graphite microstructure of GCI is widely understood to have a strong influence on the macro properties of the material [13]–[15]. GCI pipes are more vulnerable to tensile failure, due to their compressive strength being 1.3 to 4 times larger than their tensile strength [16], [17], so matching the tensile stress-strain and failure behaviour is essential. For the BS 416-2 pipe's microstructure and stress-strain behaviour to be suitable they must be similar to literature data for exhumed GCI water pipes.

The structure of this paper is as follows: firstly, available information from the literature regarding the observed microstructure and tensile stress-strain behaviour is presented; then, the methods used to assess the BS 416-2 pipe are explained; and finally, the results obtained are compared with the literature data to assess the similarity of BS416-2 pipes to exhumed GCI water pipes.

2 GCI WATER PIPE PROPERTIES FROM LITERATURE

2.1 Background

A defining feature of GCI is the microscopic graphite flakes contained within the iron's microstructure. These graphite flakes act as cracks within the material, causing GCI to demonstrate brittle tensile behaviour [14], [17]. Graphite flakes also enable graphitic corrosion, which can result in deep corrosion pits forming [18]. The size and distribution of the graphite flakes is known to strongly affect the material's mechanical properties, with larger flakes generally resulting in a lower bulk tensile strength [16]. The size and distribution of the graphite flakes is determined by the chemical composition of the GCI and the rate at which the iron cooled, with slower cooling generally allowing larger flakes to form [14]. The cooling rate can be influenced by the pipe's wall thickness, the ambient temperature, and the manufacturing process used.

GCI pipes broadly fall into two categories which are determined by the manufacturing technique used. In the UK, pit-cast iron pipes were manufactured from the mid-1800s until the 1920s using vertical sand moulds, which generally resulted in slow cooling times and larger graphite flakes. Spun-cast pipes were manufactured from the 1920s to 1960s and were cast in horizontal, spinning, water-cooled metal moulds, resulting in fast cooling times and smaller graphite flakes [1], [19]–[21]. The BS 416-2 pipe in this investigation has been produced using a spin-casting technique.

2.2 Graphite Flake Microstructure

Most previous studies report the graphite flake morphology and sizes of the GCI pipes examined according to ASTM A247-19 [22], or a preceding version of the standard. A247-19 describes the graphite microstructure according to its size, form, and distribution.

Literature data for pit-cast iron pipes give flake sizes of between Class 5 and Class 1, or 40 µm to ≥640 µm, with the large flakes tending to occur in the central region of the pipe wall [11], [14], [16]. Similar data for spun-cast pipes gives sizes between Class 8 and Class 4, or <10 µm to 160 µm, with the larger flakes often occurring towards the inside wall of the pipe [11], [14], [16].

These size ranges therefore broadly match the theory that pit-cast pipes should have larger flakes than spun-cast pipes. The trends across the pipe walls also suggest that the centre of the wall cools most slowly in pit-cast pipes, whereas the inside wall cools most slowly in spun-cast pipes. The images in Figure 1 illustrate the typical difference observed in graphite flake size and distribution between pit and spun-cast pipes.

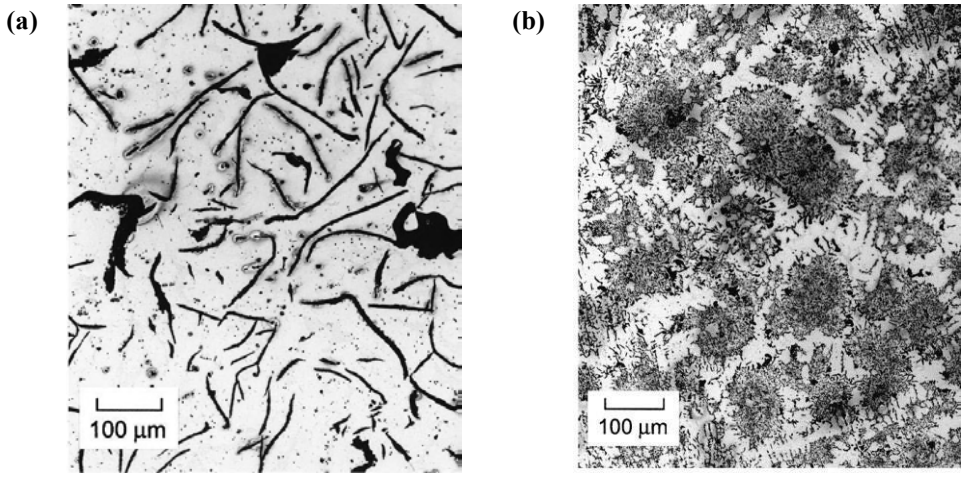

*Figure 1: Examples of **(a)** pit-cast and **(b)** spun-cast graphite microstructures from Makar and Rajani [14].*

For both pit and spun-cast pipes the graphite form reported is exclusively Type VII flake graphite, apart from one spun cast pipe inspected by Makar and Rajani [14], which featured some Type III compacted graphite at its outer edge. The authors attributed this irregularity to potential extended heat treatment.

In terms of graphite distribution, pit cast-pipes are reported to display Distributions A, B, and C (see Table 1) [11], [14], [16]. Spun-cast pipes are generally dominated by Distribution D, although Distributions A and C are often present near the inside wall of the pipe [14], [16].

Table 1: Description of ASTM graphite distributions, according to Makar and Rajani [14].

Flake Distribution	Description
A	Uniformly distributed, apparently randomly oriented flakes (see Figure 1a)
B	Rosette pattern of graphite flakes
C	Randomly oriented flakes of widely varying sized
D	Very fine pattern of flakes surrounding areas without graphite (see Figure 1b)
E	Graphite flakes have preferred orientation and appear in quasi-regular pattern

2.3 Stress-Strain Behaviour

For BS416-2 pipes to be a suitable alternative to exhumed GCI water pipes in the planned small-scale fatigue experiment, the BS416-2 pipe must demonstrate similar tensile stress-strain and failure behaviour to that observed in ex-service water pipes. The BS416-2 pipe investigated is spun-cast so literature stress-strain data from exhumed spun-cast pipes is the focus here. Key numerical parameters to consider in this assessment are the yield stress, tensile failure stress and strain, and the initial elastic modulus. The general shape of the material tensile stress-strain curve must also be similar.

Literature reports of stress-strain tests using exhumed GCI pipes come mainly from North America and Australia, and are predominantly for spun-cast pipes [9], [14]–[17]. Unfortunately, few stress-strain curves are available in the literature, so box-plots of the available tensile stress-strain parameters for spun-cast pipes are provided in Figure 2. The spread of Ultimate Tensile Strengths (UTSs) observed for spun-cast pipes is significant with a range of 130.0 to 304.9 MPa. Previous authors have attributed this spread to the fact that only minimum requirements for UTS were specified by standards for GCI water pipe manufacture, resulting in significant scatter above these lower limits [17], [23]. It is worth noting that, as expected from the microstructural differences, pit-cast pipes are generally observed to have lower tensile strengths than spun-cast pipes [14]–[16].

Failure strains are less frequently reported by literature sources, however Makar and McDonald [16] concluded from their tests that spun-cast pipes generally have higher failure strains than pit-cast pipes. The same study also found that the stress-strain response of spun-cast GCI often features a "knee" (see Figure 7, 'SC2 representative curve'), indicating a degree of plastic yielding, whereas pit-cast material does not. As a result, the 0.2% offset yield strength can be calculated for some spun-cast pipes, as shown in Figure 2. Regarding the elastic stress-strain response, spun-cast pipes generally seem to have higher initial elastic moduli than pit-cast pipes [15], [16].

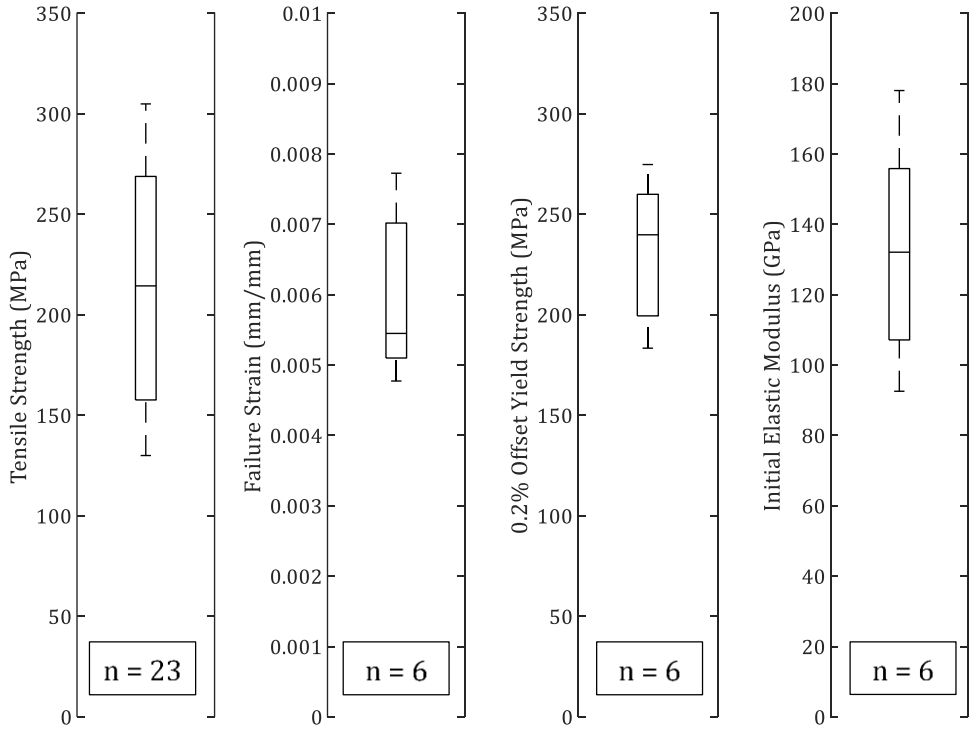

Figure 2: Box plots of the spun-cast GCI water pipe tensile stress-strain data available from the literature [9], [14]–[17].

3 METHODOLOGY

3.1 Materials

A 3000 mm long, 50 mm nominal diameter BS 416-2 soil pipe (product code MS2001 [24]) manufactured by Hargreaves Foundry (Halifax, UK) was obtained so that the properties of the pipe could be characterised and compared with the literature data for exhumed GCI water pipes. DN50 was selected because these pipes are intended for use in scaled-down tests where a small diameter is beneficial.

The measured outside diameter of the pipe averaged 58.11 mm, and the wall thickness averaged 3.54 mm. The manufacturer confirmed via private communication that the pipe supplied was manufactured using a centrifugal casting process (spin-casting) in a water-cooled metal mould. The pipe was supplied with internal and external coatings of epoxy resin, visible in Figure 3, which were removed by grit-blasting.

3.2 Microscope Inspection

The microscope inspection aimed to characterise the graphite microstructure of the material across the full thickness of the pipe wall. Three small material samples were cut from the BS416-2 pipe and mounted in Bakelite so that the circumferential cross-section was visible, as shown by Figure 3. The mounted samples were then ground using P280, P800, and P1200 grit paper. Following this the samples were polished using 9 µm then 3 µm diamond paste, and lastly 0.05 µm aluminium oxide.

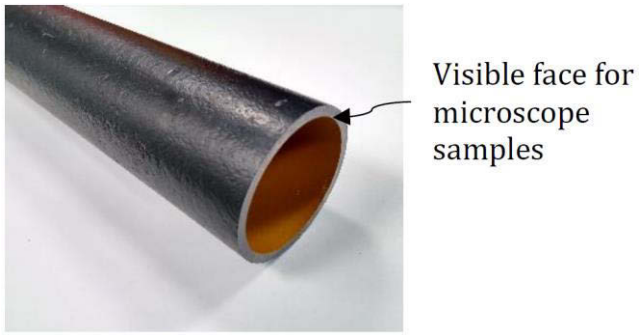

Figure 3: Image of a BS416-2 soil pipe showing the face selected for microscope inspection.

ASTM standard A247-19 [22] was adhered to for evaluation of the graphite microstructure. As a result, microscope images were taken at x100 magnification. To capture the expected variation in flake size across the pipe wall, a series of images were taken, spanning in a straight line from the outside wall to the inside wall. This was repeated for three separate samples, with a total image count of 21 for the first sample and 33 each for the second two samples. The intervals between the images for a given specimen were approximately equal.

Each image was processed using the MatLab Image Processing Toolkit to determine the length and area of the graphite present. A247-19 [22] does not specify the process for measuring flake length, so the largest straight line distance between any pair of points around the flake edge was used. Objects smaller than 1 µm were excluded as it was not possible to confirm whether these were graphite or other features due the resolution of the images. The results from the three samples were combined to provide a more representative view of the pipe's graphite microstructure.

3.3 Tensile Testing

As recommended by ASTM E8/E8M [25] for characterising the UTS of large diameter tubular products, a specimen was cut from the wall of the BS 416-2 pipe with the geometry shown by

Figure 4. Five specimens were cut from the same length of pipe as the microscope samples using wire-EDM cutting.

The specimens were tested to failure using a Shimadzu 300 kN electronic test machine. Grips with curved inserts were made so the specimens could be held securely without crushing the curved end sections. A 50 mm extensometer was fitted to the gauge section of the specimens during testing to record extension. Upon failure, the thickness and width of the fracture surface was measured manually using digital callipers. These measurements were used to calculate the cross-sectional area at the point of failure, which was in turn used to calculate the applied stress.

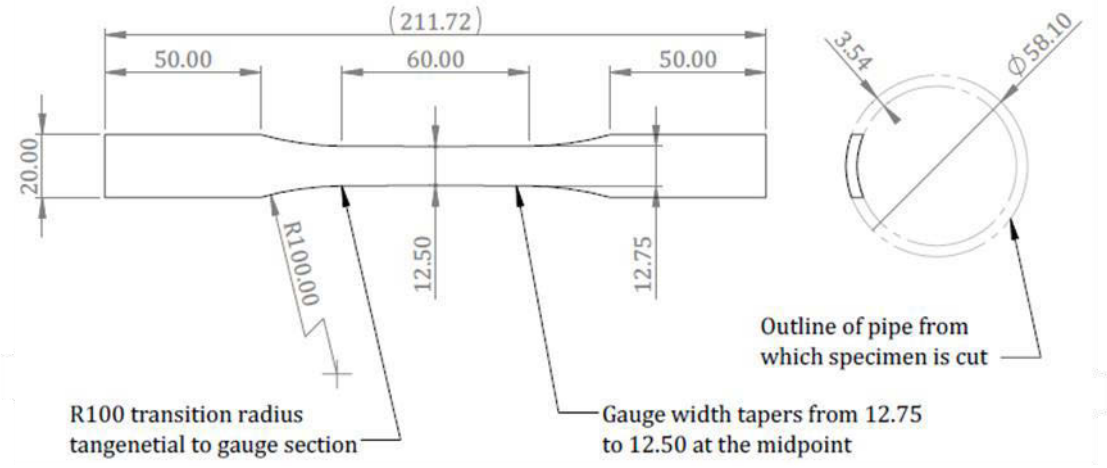

Figure 4: Tensile specimen design used for characterising the UTS of the BS 416-2 DN50 pipe. 3rd angle projection, not to scale.

4 RESULTS AND DISCUSSION

4.1 Graphite Microstructure

The majority of graphite observed in the BS416-2 pipe fell into ASTM size Class 8 (<10 μm), with some larger Class 7, 6, and 5 flakes also present. As shown by Figure 5, the breakdown of graphite size was found to be very similar for the two quarters of the wall closest to the outside surface, with size Class 8 graphite making up around 85% of the total graphite area, and slightly more than 1% of the area being Class 6. The largest graphite was found to occur closer to the inside wall, with about 3.5% of the graphite area in the wall quarter closest to the inside edge being Class 5. The largest individual piece of graphite observed in this region was 76.6 μm long. These results are in agreement with the literature values for spun cast pipes reported above where size Class 8 to 4 were observed, with the larger graphite tending to occur towards the pipe inside wall.

The graphite observed in the BS416-2 pipe was mainly Type VII flake graphite (see Figure 6), with a small amount of Type III compacted graphite present near the inside wall of the pipe. Where Type III graphite occurred it was mainly found near regions of iron devoid of graphite, such as the example shown in Figure 6d. Note that in the top region of Figure 6d the faint white lines may indicate the presence of pearlite. The dominance of Type VII flake graphite is expected for a spun-cast GCI water pipe, based on the literature review findings, however the occurrence of Type III compacted graphite near the pipe inside wall is more unusual and is perhaps linked to the presence of the suspected pearlite grains.

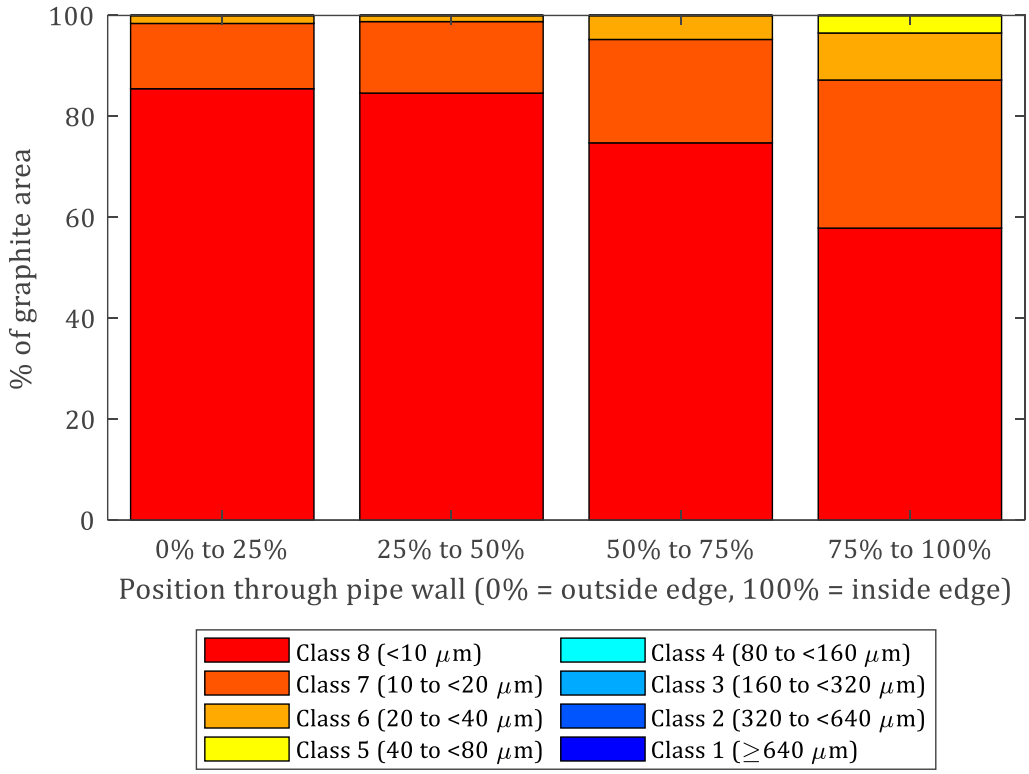

Figure 5: Proportion of graphite, by area, in each ASTM size class across the wall of the BS 416-2 DN50 pipe.

Nearly all observations made in the mid-region of the pipe wall showed Distribution D graphite (see Figure 6b). Around 10% of observations near the outside wall and more than 60% of the observations near the inside wall were Distribution A or C (Figure 6a and 6c). These observed distributions match those expected for a spun-cast GCI, based on the literature review above. This can be seen visually by comparing Figure 1b with Figure 6b, although the difference in scale must be noted.

In summary, the graphite sizes, types, and distributions observed in the BS416-2 pipe match the literature data for spun-cast water pipes well. The outer and middle regions of the pipe wall are dominated by fine (Class 8 and Class 7), Distribution D, Type VII graphite flakes (Figure 6b) which are typical of spun-cast pipes examined by previous authors [14], [17]. The region of cast iron closest to the inside wall of the pipe varied from this norm, with ~500 µm diameter patches of Distribution A or C, Type VII flakes with sizes up to Class 5 (Figure 6c). These areas with large flake sizes are likely due to the longer cooling time experienced by the iron closest to the inside wall, giving more time for larger flakes to form, and are consistent with observations in the literature [14], [17]. Also found close to the inside wall were possible areas of pearlite, surrounded by Type III compacted graphite (Figure 6d). Pearlite grains are associated with cast iron that has cooled more slowly [14] and Type III graphite is reportedly common in annealed malleable iron castings [22]. Therefore, the occurrence of the regions containing pearlite and Type III graphite is also probably associated with the slower cooling rate of the pipe inside wall.

(a) ~1% – Type VII, Distribution A/D, Class 7-8

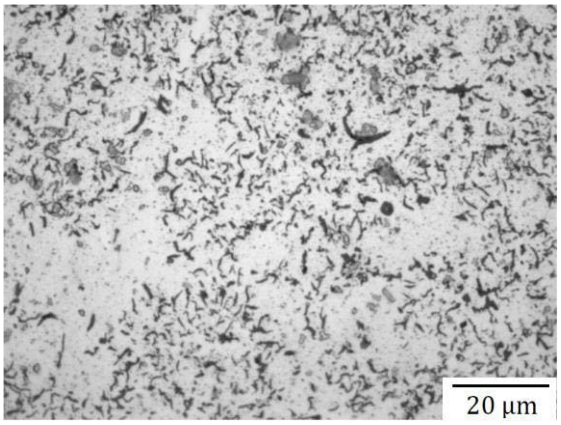

(b) ~50% – Type VII, Distribution D, Class 7-8

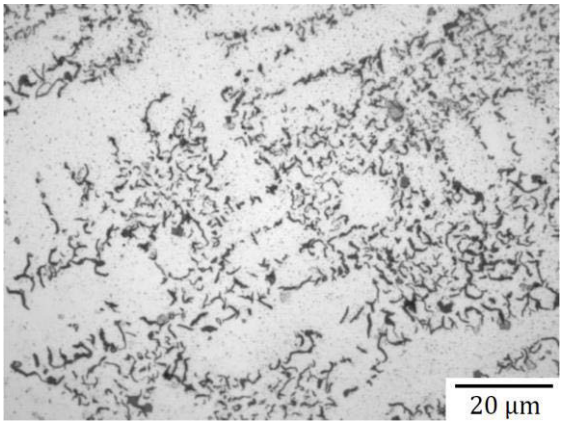

(c) ~90% – Type VII, Distribution C, Class 5-8

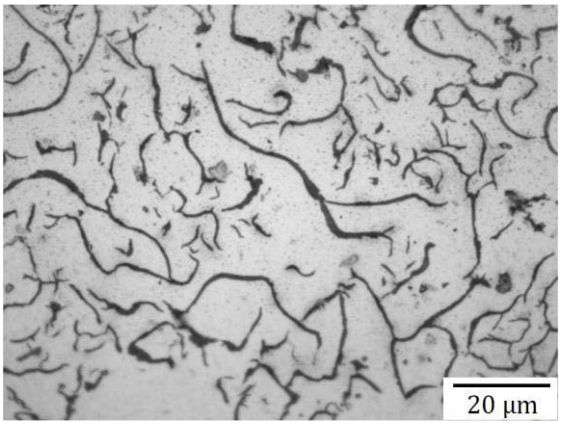

(d) ~95% – Type III/VIII, Distribution D, Class 7-8

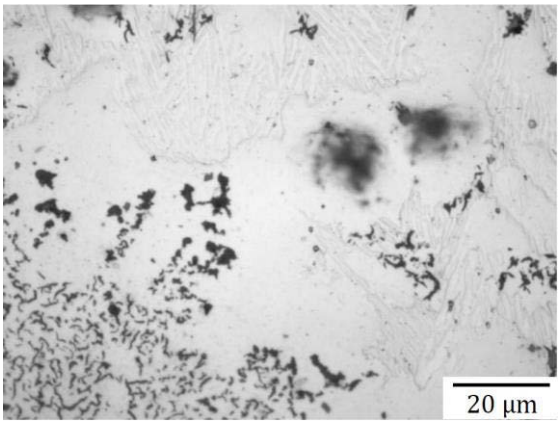

Figure 6: Selection of x100 magnification images showing the graphite microstructure of the BS416-2 pipe. ~X% refers to the approximate position of the image, where ~0% would be the outside wall and ~100% would be the inside wall.

4.2 Stress-Strain Behaviour

The stress-strain results of the five tensile specimens tested are shown in Figure 7. From these stress-strain curves the initial elastic modulus, failure stress and failure strain were determined; these values are provided in Table 2. The 0.2% offset yield stress could not be calculated for any of the BS416-2 specimens as failure occurred before the offset slope was met.

The average initial elastic modulus of the five specimens was found to be 126 GPa, with a range of +13% -9%. This spread is quite large considering that the five specimens were cut from the same section of the same pipe, however, this is expected for GCI. Repeated tensile tests of the same type of specimen cut from the same spun-cast pipes by Makar and McDonald [16] returned elastic moduli ranging between 114 GPa and 184 GPa for one pipe (approximately ±23%), and between 78 GPa and 167 GPa for the other (approximately ±36%). The cause of this variation in elastic modulus within the same pipe is likely due to local differences in microstructure, as observed during the microscope investigation. The BS416-2 pipe elastic modulus measurements all fall well within the range of values reported in the literature for spun-cast water pipes.

The average tensile strength of the five BS416-2 specimens was 292 MPa, with a range of +4.8% -4.5%. This spread is also considerably less than the range of +20% -22% observed by Makar and McDonald [16] for seven identical specimens cut from one ex-service spun cast pipe with an

average tensile strength of 213 MPa (Figure 7, 'SC2 9mm thick specimen failure points'). The tensile strengths measured for the BS416-2 pipe are close to the highest tensile strengths reported for spun-cast pipes in literature, falling within or just above the 95th percentile (see Figure 2). Thinner GCI castings are known to demonstrate higher tensile strengths, even when the same molten iron mixture is used [26]. The BS416-2 pipes have a wall thickness of around 3.54 mm whereas the pipes tested in the literature generally had wall thicknesses between 8 mm and 12.7 mm. Therefore, the thinner walls of the BS416-2 pipe is likely the cause of the relatively high tensile strength measured.

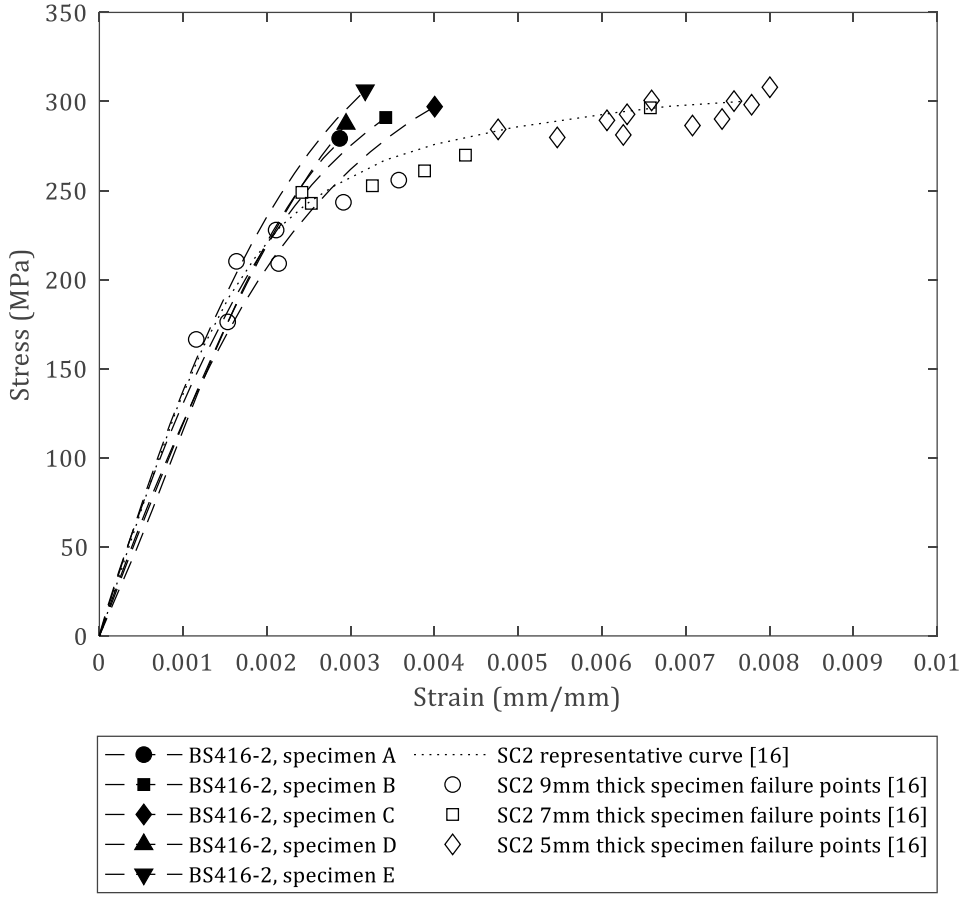

Figure 7: Tensile stress-strain curves for the five BS416-2 pipe tensile specimens tested as part of this work. The representative stress-strain curve and individual test failure points for spun-cast pipe "SC2" from [16] are provided for comparison.

Table 2: BS416-2 tensile stress-strain parameters for each of the five specimens tested as part of this work.

Specimen	Initial E (GPa)	UTS (MPa)	Failure Strain (mm/mm)
A	115	279	0.0029
B	134	291	0.0034
C	121	297	0.0040
D	120	287	0.0029
E	142	306	0.0032

The average failure strain of the BS416-2 pipe specimens was 0.0033, with a range of +21% -12%. As with the other results, this spread is much smaller than that observed by Makar and McDonald [16] for similar tests. The magnitude of the failure strain is lower than the failure strains reported in the literature for spun-cast pipes, the smallest literature value being around 0.005 (see Figure 2). However, these literature values are usually from the strongest specimens tested from each pipe which the references highlight as representative [15], [16]. Fortunately, Makar and McDonald [16] provide the data from repeats for one of the spun-cast pipes they investigated, "SC2", and these values are plotted on Figure 7. These repeats show a huge variation in failure strain with some specimens displaying ductile behaviour, while others are very brittle. Generally, Makar and McDonald [16] found that specimens which included nearly the full wall thickness (9mm thick) were more brittle, and failed at lower strains, whereas specimens that had the inside wall material removed (5mm thick) were more ductile and demonstrated higher failure strains. The BS416-2 tensile specimens tested in the present work included the full wall thickness, so their brittle behaviour matches Makar and McDonald's [16] observations for the 9mm thick specimens, which also included most of the wall thickness. A possible cause of Makar and McDonald's thinner specimens demonstrating more ductile behaviour than the full wall specimens is that the material removed during thinning contained the largest graphite flakes; in other words, thinning the specimens probably removed the largest internal defects.

In summary, for applied stresses below 200 MPa the BS416-2 pipe's tensile stress-strain matches literature data for spun-cast pipes well. The failure behaviour is much more brittle than the "representative" stress-strain curves for spun-cast pipes provided in the literature which show more ductile behaviour [15]–[17]. However, closer examination of these literature results shows that more brittle behaviour can occur when the whole pipe wall is sampled, as is the case for the tests conducted for the present work. The magnitude of the pipe's tensile strength is high compared to the literature data, but this is likely to be a result of the BS416-2 pipe's thinner walls. It is also clear that further work is required to fully characterise and understand the complex and highly variable material that is spun-cast grey iron.

5 CONCLUSIONS

The graphite microstructure and tensile stress-strain behaviour of an off-the-shelf BS416-2 soil pipe were characterised and compared with literature data for spun-cast GCI water pipes. The motivation behind this work was that a large number of small-diameter, un-corroded GCI pipes are needed for a planned fatigue experiment. Through the comparisons performed it was concluded that BS 416-2 soil pipes can be used to represent spun-cast GCI water pipes in small-scale destructive experiments. Future work will aim to characterise the compressive stress-strain and fatigue behaviour of these BS416-2 pipes.

6 ACKNOWLEDGEMENTS

This work was funded by UK Water Industry Research (UKWIR) and the ESPRC through the Water Infrastructure and Resilience (WIRe) Centre for Doctoral Training. The authors would like to thank Dennis Dellow from UKWIR for providing an experienced industry perspective on the project. Also a special thanks to the technicians Paul Blackbourne, Sam Gibson, Geoffrey Hibberd, and Tesoro Monaghan for their work which enabled the microscopy and tensile testing to take place. For the purpose of open access, the author has applied a creative commons attribution (CC BY) license to any author accepted manuscript versions arising.

7 REFERENCES

[1] N. A. Barton, T. S. Farewell, S. H. Hallett, and T. F. Acland, “Improving pipe failure predictions: Factors effecting pipe failure in drinking water networks,” Water Research, vol. 164, p. 114926, 2019, doi: 10.1016/j.watres.2019.114926.

[2] S. Rathnayaka, B. Shannon, C. Zhang, and J. Kodikara, “Introduction of the leak-before-break (LBB) concept for cast iron water pipes on the basis of laboratory experiments,” Urban Water Journal, 2017, doi: 10.1080/1573062X.2016.1274768.

[3] M. Larson and L. Jönsson, “Elastic Properties of Pipe Materials during Hydraulic Transients,” Journal of Hydraulic Engineering, vol. 117, no. 10, pp. 1317–1331, 1991, doi: 10.1061/(asce)0733-9429(1991)117:10(1317).

[4] D. Chan, C. P. K. Gallage, P. Rajeev, and J. Kodikara, “Field performance of in-service cast iron water reticulation pipe buried in reactive clay,” Canadian Geotechnical Journal, 2015, doi: 10.1139/cgj-2014-0531.

[5] C. Randeniya, D. J. Robert, C. Q. Li, and J. Kodikara, “Large-scale experimental evaluation of soil saturation effect on behaviour of buried pipes under operational loads,” Canadian Geotechnical Journal, vol. 57, no. 2, pp. 205–220, 2020, doi: 10.1139/cgj-2018-0544.

[6] H. Rezaei, B. Ryan, and I. Stoianov, “Pipe failure analysis and impact of dynamic hydraulic conditions in water supply networks,” Procedia Engineering, vol. 119, no. 1, pp. 253–262, 2015, doi: 10.1016/j.proeng.2015.08.883.

[7] Department for Transport, “AADF Data - major and minor roads,” Gov.uk, 2020. https://roadtraffic.dft.gov.uk/downloads (accessed Apr. 19, 2021).

[8] W. Brevis, L. Susmel, and J. Boxall, “Investigating in-service failures of water pipes from a multiaxial notch fatigue point of view: A conceptual study,” Proceedings of the Institution of Mechanical Engineers, Part C: Journal of Mechanical Engineering Science, vol. 229, no. 7, 2015, doi: 10.1177/0954406214553020.

[9] R. Jiang, S. Rathnayaka, B. Shannon, X.-L. Zhao, J. Ji, and J. Kodikara, “Analysis of failure initiation in corroded cast iron pipes under cyclic loading due to formation of through-wall cracks,” Engineering Failure Analysis, vol. 103, pp. 238–248, 2019, doi: 10.1016/j.engfailanal.2019.04.031.

[10] D. A. Jesson et al., “Thermally induced strains and stresses in cast iron water distribution pipes: An experimental investigation,” Journal of Water Supply: Research and Technology - AQUA, 2010, doi: 10.2166/aqua.2010.078.

[11] H. Mohebbi, D. A. Jesson, M. J. Mulheron, and P. A. Smith, “The fracture and fatigue properties of cast irons used for trunk mains in the water industry,” Materials Science and Engineering A, 2010, doi: 10.1016/j.msea.2010.05.071.

[12] British Standards Institution, “Discharge and ventilating pipes and fittings , sand-cast or spun in cast iron - Part 2: Specifications for socketless systems. BS 416-2:1990.” British Standards Publications, 1990. [Online]. Available: https://bsol-bsigroup-com.sheffield.idm.oclc.org/Bibliographic/BibliographicInfoData/000000000000225830

[13] P. A. Blackmore and K. Morton, “Structure-property relationships in graphitic cast irons,” International Journal of Fatigue, vol. 4, no. 3, pp. 149–155, 1982, doi: 10.1016/0142-1123(82)90042-1.

[14] J. M. Makar and B. Rajani, “Gray Cast-Iron Water Pipe Metallurgy,” Journal of Materials in Civil Engineering, 2000, doi: 10.1061/(asce)0899-1561(2000)12:3(245).

[15] H. M. S. Belmonte, M. Mulheron, and P. A. Smith, “Weibull analysis, extrapolations and implications for condition assessment of cast iron water mains,” Fatigue and Fracture of Engineering Materials and Structures, 2007, doi: 10.1111/j.1460-2695.2007.01167.x.

[16] J. M. Makar and S. E. McDonald, “Mechanical Behavior of Spun-Cast Gray Iron Pipe,” Journal of Materials in Civil Engineering, vol. 19, no. 10, pp. 826–833, 2007, doi: 10.1061/(ASCE)0899-1561(2007)19.

[17] M. v. Seica and J. A. Packer, “Mechanical Properties and Strength of Aged Cast Iron Water Pipes,” Journal of Materials in Civil Engineering, 2004, doi: 10.1061/(asce)0899-1561(2004)16:1(69).

[18] R. Logan et al., “Graphitic corrosion of a cast iron trunk main: Implications for asset management,” 2014. doi: 10.2495/UW140351.

[19] UKWIR, “Water Industry Information & Guidance Note: Ductile Iron Pipes and Fittings,” 2006. [Online]. Available: https://www.water.org.uk/wp-content/uploads/2018/11/ign-4-21-01.pdf

[20] British Standards Institution, "Specification for cast iron pipes and special castings for water, gas and sewage. BS 78:1917." British Standards Publications, London, 1917. [Online]. Available: https://bsol.bsigroup.com/Bibliographic/BibliographicInfoData/000000000030338181

[21] British Standards Institution, "Centrifugally cast (spun) iron pressure pipes for water, gas & sewage. BS 1211:1958." British Standards Publications, London, 1958. [Online]. Available: https://bsol.bsigroup.com/Bibliographic/BibliographicInfoData/000000000000034043

[22] ASTM International, "Standard Test Method for Evaluating the Microstructure of Graphite in Iron Castings A247-19." ASTM Compass, West Conshohocken, PA, USA, 2019. doi: 10.1520/A0247-19.

[23] B. Rajani and J. Makar, "A methodology to estimate remaining service life of grey cast iron water mains," Canadian Journal of Civil Engineering, 2000, doi: 10.1139/l00-073.

[24] Hargreaves Foundry, "Mech 416 Cast Iron Mechanically Jointed Soil System," www.hargreavesfoundry.co.uk, 2021. https://www.hargreavesfoundry.co.uk/cast_iron_drainage/mech416/ (accessed Sep. 06, 2021).

[25] ASTM International, "Standard test methods for tension testing of metallic materials ASTM E8/E8M - 16a." ASTM Compass, West Conshohocken, PA, USA, 2016. doi: 10.1520/E0008.

[26] British Standards Institution, "Founding - Grey cast irons. BS EN 1561:2011." British Standards Publications, 2011. [Online]. Available: https://bsol-bsigroup-com.sheffield.idm.oclc.org/Bibliographic/BibliographicInfoData/000000000030214938